Journal of Nuclear Materials 600 (2024) 155291

Contents lists available at ScienceDirect

Journal of Nuclear Materials

journal homepage: www.elsevier.com/locate/jnucmat

Short communication

Predictive phase stability of actinide-bearing hollandite waste forms from first-principles calculations

Amir M. Mofrad [a,b,*], Matthew S. Christian [a,b,c,1], Juliano Schorne-Pinto [a,b], Jake Amoroso [a,d], Kyle S. Brinkman [a,f], Hans-Conrad zur Loye [a,e,d], Theodore M. Besmann [a,b]

[a] Center for Hierarchical Waste Form Materials, Columbia, SC 29208, USA
[b] Department of Mechanical Engineering, University of South Carolina, Columbia, SC 29208, USA
[c] Sandia National Laboratory, Albuquerque, NM 87185, USA
[d] Savannah River National Laboratory, Aiken, SC, USA
[e] Department of Chemistry and Biochemistry, University of South Carolina, Columbia, SC 29208, USA
[f] Department of Materials Science and Engineering, Clemson University, Clemson, SC 29634, USA

ARTICLE INFO

Keywords:
Hollandite
Tunnel structure
Nuclear waste form
Density functional theory

ABSTRACT

In this work, we investigated the stability trends of actinide-bearing hollandites using density functional theory calculations. Incorporating actinides generally decreased the stability of cesium end-members relative to their barium equivalents. Among the actinides, neptunium-containing structures were consistently the least stable. Curium was the most stable actinide in the +3 oxidation state, followed by americium, plutonium, uranium, and neptunium. Conversely, in the +4 state, uranium-bearing hollandites were the most stable. An inverse correlation between actinide content and stability was consistently observed.

Treating the high-level legacy nuclear waste materials remaining from decades of defense programs and converting them into long-term waste forms continues to be a significant challenge [1]. Among the radionuclides requiring safe sequestration, ^{137}Cs, a fission product with a half-life of ≈ 30 years, demands special attention due to its significant toxicity and mobility, which pose a potential threat to the biosphere [2,3]. In addition, the β decay and thus the transmutation of cesium to stable barium can affect the stability of the waste form materials [4].

Borosilicate glass is widely recognized as the most accepted waste form for immobilizing nuclear waste products, thanks to its ability to capture a wide range of radioactive (and non-radioactive) elements, as well as its high chemical durability [5]. However, the inferior thermal stability of borosilicate glass compared to crystalline materials motivates the development of alternative waste forms with improved performance and properties [6]. One effective method for radioactive cesium treatment is to reduce its solubility by fixing it in a crystalline phase in SYNROC [2,7,8], which is a multi-phase composite of distinct phases, each of which is compositionally tailored to immobilize specific isotopes by incorporation into a crystalline lattice [9]. SYNROC phases can immobilize a significant amount of ^{137}Cs, possess high thermal stability, and exhibit low solubility, which reduces the risk of leaching over repository time scales [10].

A prominent and distinct titanate phase in SYNROC is hollandite [11], which is usually denoted as A_x $(Ti^{4+},B)_8O_{16}$, where A can be an alkali and/or alkaline earth cation, and B is a di-, tri-, tetra-, or penta-valent cation [10,12]. Due to the structural flexibility, a wide range of compositional variations is possible for hollandites [13]. Fig. 1 shows the typical crystal structure of the hollandite phase, having edge and corner sharing TiO_6 octahedra that form a framework consisting of tunnels parallel to the c-axis ([001] direction). There are eight sites for these octahedra (B-sites), and there are two available A-sites. However, A-site occupancy is dictated by charge balance requirements and thermodynamic stability [9,15,16].

Immobilizing radioactive waste using hollandites has been the subject of significant research thanks to hollandite's high phase stability and resistance to leaching. Studies, such as those by Xu et al. [17] on gallium-bearing hollandite have provided insights into the structural stability and ion mobility of these materials demonstrating the effective immobilization of alkali cations with high concentrations of cesium

* Corresponding author at: Department of Mechanical Engineering, University of South Carolina, Columbia, SC 29208, USA.
E-mail address: amirmehdi.mofrad@sc.edu (A.M. Mofrad).
[1] Present affiliation: Sandia National Laboratory, Albuquerque, NM, 87185, USA.

https://doi.org/10.1016/j.jnucmat.2024.155291
Received 18 April 2024; Received in revised form 10 June 2024; Accepted 10 July 2024
Available online 14 July 2024

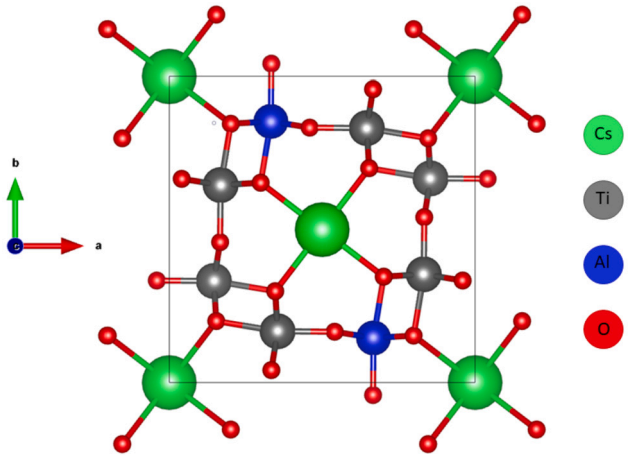

Fig. 1. Unit cell of a cesium-aluminum hollandite structure viewed along the [001] direction. Picture generated using the VESTA program [14].

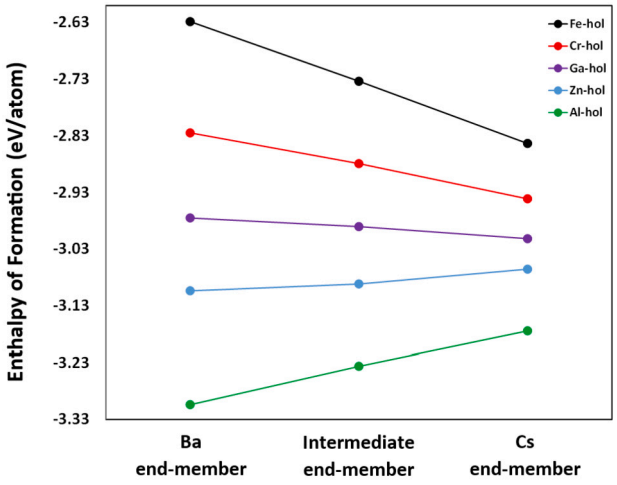

Fig. 2. Averaged DFT-calculated formation enthalpies (in eV/atom) from the elements of previously synthesized hollandites containing either solely barium or cesium as the alkali element, or an equimolar mixture of barium and cesium. The formula for each end-member is as follows: Ba end-member: $Ba_{1.33}M_{2.66}Ti_{5.34}O_{16}$, Intermediate end-member: $Ba_{0.67}Cs_{0.67}M_2Ti_6O_{16}$, and Cs end-member: $Cs_{1.33}M_{1.33}Ti_{6.67}O_{16}$, where M = Fe, Cr, Ga, Zn, and Al.

and/or barium (i.e., cesium end-member and barium end-member, respectively). Building on this, Wen et al. [18] investigated the impact of both A-site and B-site ordering on the structural stability of hollandites with compositions $Ba_xCs_y(M_{x+y/2},Ti_{8-x-y/2})O_{16}$, where $0 \leq x, y \leq 1.33$ and M = Zn^{2+}, Ga^{3+}, and Al^{3+} by means of DFT calculations, revealing that intermediate compositions containing both cesium and barium are less stable than those of the pure cesium and/or pure barium end-members.

Despite these considerable contributions to understanding hollandites, there has not been a systematic investigation of the structural stability and/or leaching resistance of these types of phases that also contain actinide elements. This is particularly of interest because hollandites can not only sequester radioactive alkali cations in the tunnels but also immobilize other radionuclides such as uranium, neptunium, plutonium, etc. in the framework, which can make them true "Hierarchical Waste Form". In addition, information available about the key properties (e.g., phase equilibria, free energies) for these structures is sparse, with little reported. To fill this knowledge gap, this work establishes the relationship between the structural stability of actinide-bearing hollandites and composition by means of DFT calculations. This is the first such study of these novel structures, providing the insights necessary to support the synthesis and experimental investigation of the materials.

This work is similar to the study by Wen et al. [18], in which the structural stabilities of barium and cesium hollandites with compositions $Ba_{1.33}Al_{2.66}Ti_{5.34}O_{16}$, $Ba_{0.67}Cs_{0.67}Al_2Ti_6O_{16}$, and $Cs_{1.33}Al_{1.33}Ti_{6.67}O_{16}$ were investigated by means of DFT calculations. We wish to investigate the question of whether or not actinides, An (i.e., U, Np, Pu, Am, and Cm) when substituted into the B-sites of hollandite phases are stable relative to previously known/synthesized hollandites. We start by calculating the enthalpy of formation of known hollandites using DFT calculations to find the maximum and minimum range enthalpy values for these hollandites. We then examine the stability of hypothetical structures in which some titanium atoms are exchanged by actinides and no other elements are added. This will be referred to as actinide-hollandites, in which actinides nominally are in the +3 oxidation states. Subsequently, we investigate another class of these hypothetical structures in which aluminum is also present, and the actinides are substituted for some of the titanium atoms. This will be referred to as aluminum-actinide-hollandites, where these heavy elements theoretically exist in the +4 oxidation state. For both of these classes we considered the barium end-member, cesium end-member, and intermediate end-member (Cs/Ba = 1) structures. For all the calculations a $1 \times 1 \times 3$ supercell was used to reflect the above compositions. The details of how the actinide and/or aluminum atoms are distributed in the model are provided in Ref. 18.

The crystal structure of aluminum-hollandite with tetragonal symmetry was used to construct the hypothetical compounds [19]. To calculate the enthalpy of formation from the elements (at 0 K), electronic structure calculations were performed using DFT [20,21]. When unpaired electrons were present, spin polarized calculations were performed as implemented in the Vienna ab initio simulation package (VASP) [22–25]. The electron–core interactions were described by projector augmented wave (PAW) potentials [26,27]. The generalized gradient approximation (GGA) with Perdew–Burke–Ernzerhof (PBE) functional was used for describing the exchange–correlation energy [28,29]. The width of Gaussian smearing was 0.02 eV. For all systems, the plane-wave kinetic cutoff energy was 520 eV so as to be consistent with both Materials Project (MP) [30] and the Open Quantum Materials Databases (OQMD) [31]. Both the internal atomic positions and the lattice constants were allowed to relax until the energy converged to $\leq 10^{-6}$ eV and the forces $\leq 10^{-2}$ eV/Å. The Brillouin zone was sampled using a Monkhorst–Pack grid [32] at the Γ point with a $2 \times 2 \times 2$ k-point mesh.

To overcome the delocalization issue of PBE as well as capture the on-site Coulombic interaction of the d- and f-electrons, the Hubbard U correction (PBE $+U$) as described by Dudarev et al. was used [33]. To be consistent with OQMD, we adopted the following Hubbard U values: 3.5 eV for Cr, 4.0 eV for Fe, and 4.0 eV for the actinides. Non-spherical contributions related to the gradient of the density in the PAW spheres was included. Lastly, we allowed the symmetry to be broken. The formation enthalpies (ΔH_f) were calculated using the following equations,

$$\Delta H = E_{\text{total}} - \sum_i \mu_i x_i \quad (1)$$

where, E_{total} is the total energy of the compound, μ_i is the fitted atomic (chemical) potential of element i from OQMD, and x_i is the quantity/mole fraction of the element i in the compound. To reliably predict the phase stability of actinide-bearing hollandites, we need to compare the DFT-calculated formation enthalpies of hollandites that have been previously studied and synthesized. Fig. 2 shows the averaged formation enthalpies from elements for the Fe-, Cr-, Ga-, Zn-, and Al-hollandites calculated from first-principles. Each value represents the mean enthalpy of various configurations obtained by permutating A-site and B-site atoms, with consistently low standard deviations across calculations. All of the structures shown in this figure have been previously synthesized [19,34–36]. When examining stability trends based on alkali content, it is evident that the Cs end-member is more stable

Table 1
Comparison between the averaged DFT-calculated and experimental formation enthalpies of the previously synthesized hollandites. The experimental values are taken from Refs. 36,35,34,9,19.

	Ba end-member		Intermediate end-member		Cs end-member	
	DFT	Exp.	DFT	Exp.	DFT	Exp.
Fe-Hollandite	-2.628	-2.891	-2.734	-2.940	-2.844	-2.988
Cr-Hollandite	-2.825	-3.091	-2.879	N/A	-2.941	-3.109
Ga-Hollandite	-2.975	-3.002	-2.991	-3.021	-3.012	-3.051
Zn-Hollandite	-3.104	-3.136	-3.092	-3.127	-3.066	-3.112
Al-Hollandite	-3.304	-3.353	-3.236	-3.292	-3.174	N/A

in the Fe- and Cr-hollandites, while the Ba end-member displays greater stability in the Zn- and Al-hollandites. For the Ga-hollandite, the alkali content does not have any discernible effect on the stability. Among the structures studied, the Al-hollandite emerges as the most stable, whereas the Fe-hollandite is found to be the least stable. The observed trend in the stability can be attributed to the differences in ionic radii as well as to the amount of B-site element in the structure. According to Shannon's ionic radii data, Al(III) exhibits the smallest ionic radius (0.535 Å), while Fe(III) has the largest ionic radius at 0.645 Å. Zn-hollandite is identified as the second most stable structure, despite Zn(II)'s larger radius of 0.74 Å. This is attributed to its +2 oxidation state and the fact that, within each end-member, there is less zinc present compared to other hollandites.

The maximum and minimum ranges of DFT-calculated formation enthalpies for different end-members in Fig. 2 are as follows: Ba end-member from −2.628 to −3.303, intermediate end-member −2.734 to −3.236, and Cs end-member from −2.844 to −3.174 eV/atom. Therefore, we presume that if the predicted formation enthalpies of actinide-bearing hollandites fall within these ranges, their successful synthesis can be achieved. Due to the underbinding nature of the PBE functional, we assume that all of the calculated formation enthalpies are underestimated compared to experimental values. However, the trend in stability with respect to the elemental content predicted by DFT produces the same trend that is experimentally observed (Table 1).

The averaged DFT-calculated formation enthalpies (from elements) of the actinide-hollandites are shown in Fig. 3. The most stable hollandite is the Cm-hollandite while the Np-hollandite is the least stable. When examining stability trends based on alkali content, no specific trend is evident, meaning, for Pu-, Am-, and Cm-hollandites, the Cs end-member is found to be less stable, while for U- and Np-hollandites, the Cs end-member demonstrates greater stability compared to the Ba end-member. Here the stability trend is also justified based on the ionic radii of the actinides that are present in the structure, that is, U-hollandite has the largest ionic radius (formally +3 oxidation state), and therefore is the least stable structure, while Cm-hollandite exhibits the smallest ionic radius, and is thus the most stable structure. Comparing the predicted formation enthalpies for the actinide-hollandites to compositions previously synthesized, shown in Table 1, illustrates that it should be possible to synthesize all these structures.

Since the aluminum hollandite exhibited the highest stability compared to other elements in Fig. 2, we have considered aluminum to be present along with the actinide elements. The DFT-predicted formation enthalpies of these hollandites are shown in Fig. 4. The formulae for the compounds under consideration are $Cs_4Al_4An_8Ti_{12}O_{48}$ (represented as $Cs_{1.33}Al_{1.33}An_{2.67}Ti_4O_{16}$) and $Ba_4Al_8An_4Ti_{12}O_{48}$ (represented as $Ba_{1.33}Al_{2.67}An_{1.33}Ti_4O_{16}$). When comparing the stability of the two compounds, the Ba end-member is more stable than the cesium end-member, which can be attributed to the fact that the barium end-member has a lesser quantity of actinide in its structure, since a higher proportion of actinide generally results in decreased stability. Specifically, among the variants, the uranium hollandite, characterized by a (formally) U^{4+} oxidation state, stands out as the most stable structure. Comparing these results with values in Table 1, it is expected that all these structures can be successfully synthesized.

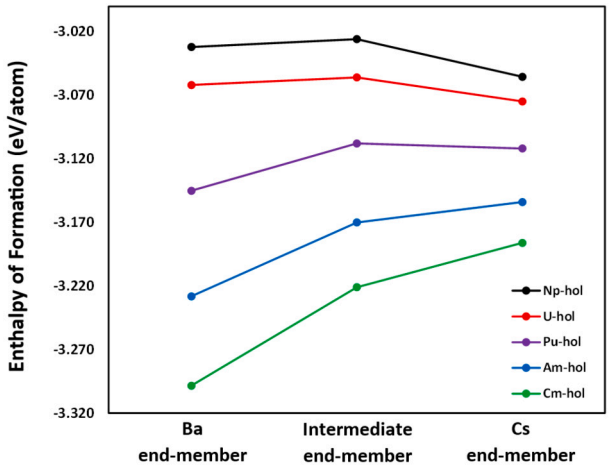

Fig. 3. Averaged DFT-calculated formation enthalpies (in eV/atom) from the elements of the actinide-hollandites containing solely barium or cesium as the alkali element, or an equimolar mixture of barium and cesium. The formula for each end-member is as follows: Ba end-member: $Ba_{1.33}An_{2.66}Ti_{5.34}O_{16}$, Intermediate end-member: $Ba_{0.67}Cs_{0.67}An_2Ti_6O_{16}$, and Cs end-member: $Cs_{1.33}An_{1.33}Ti_{6.67}O_{16}$, where An = U, Np, Pu, Am, and Cm.

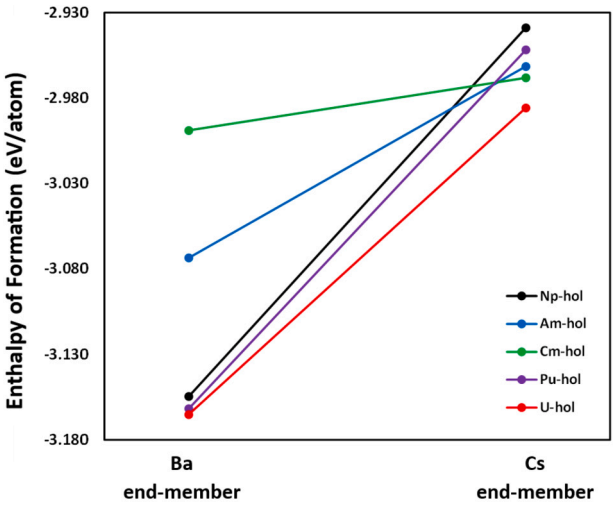

Fig. 4. Averaged DFT-calculated formation enthalpies (in eV/atom) from the elements of the aluminum-actinide-hollandites as a function of alkali content. The formula for each end-member is as follows: Ba end-member: $Ba_{1.33}Al_8An_{1.33}Ti_4O_{16}$ and Cs end-member: $Cs_{1.33}Al_{1.33}An_{2.67}Ti_4O_{16}$, where An = U, Np, Pu, Am, and Cm.

Furthermore, we explored intermediate end-members under two scenarios. The first scenario examined compositions with a 1:1 ratio of aluminum to actinide: $Cs_{0.67}Ba_{0.67}Al_1An_1Ti_6O_{16}$. The second scenario maintained the aluminum content while varying the actinide content, yielding a formula of $Cs_{0.67}Ba_{0.67}Al_2An_xTi_{6-x}O_{16}$. Our stability findings for the 1:1 ratio revealed an essentially progressive increase in the sta-

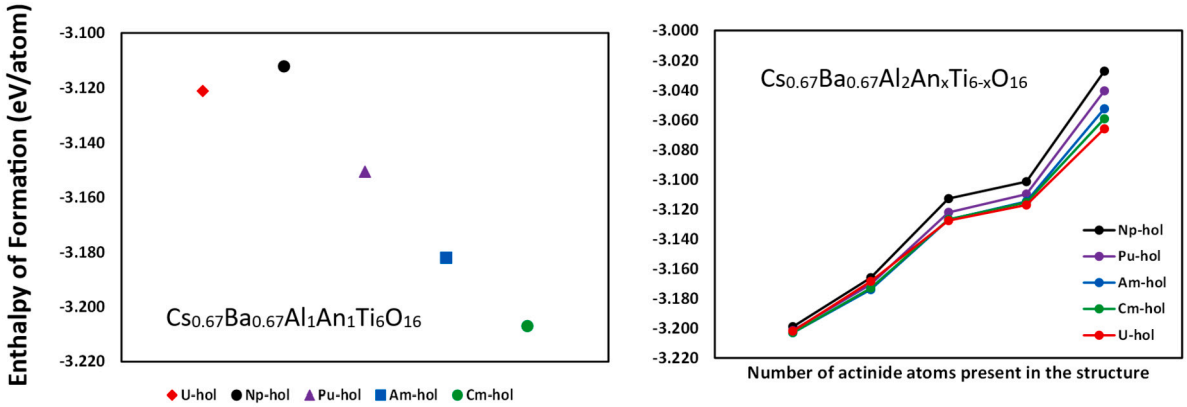

Fig. 5. Averaged DFT-calculated formation enthalpies (in eV/atom) from elements of the aluminum-actinide-hollandites as a function of alkali content. An corresponds to U, Np, Pu, Am, and Cm.

bility from U to Cm, influenced by the (formally) +3 oxidation states of the actinides and the sequential decrease in ionic radii from U to Cm. For the situations with varying actinide content, U-hollandite proved to be the most stable structure. A notable trend was the reduction in stability as the actinide content increased. Encouragingly, a comparison between the values in Table 1 and those shown in Fig. 5 corroborated the feasibility of synthesizing these structures as well.

This work for the first time predicts the existence of a new type of "hierarchical" waste form by means of density functional theory (DFT) calculations. Actinide dopants substituting for titanium in the oxygen octahedra framework were investigated along with cesium occupying the "tunnel" sites in the hollandite structure were shown to be stable and serve as guide for new experimental synthesis routes and waste form strategies. Based on the calculated values, it is evident that the cesium end-members often exhibit less stability when compared against barium end-member counterparts. A particular point of interest is the observation regarding neptunium structures. Among all the actinides considered in this work, these structures consistently ranked as the least stable. In addition, it was revealed that for the actinide-hollandites (An^{3+}), Cm-hollandite was the most stable structure, followed by Am-, Pu-, U-, and Np-hollandite. Conversely, for the aluminum-actinide-hollandite (An^{4+}), uranium-bearing hollandites consistently emerged as the most stable variants. Another consistent trend across this study was the inversely proportional relationship between actinide content and structural stability, a greater actinide content typically resulted in decreased stability. Attempts to provide more insight into these energetic relationships in the future will require efforts that focus on calculating the enthalpy of formation of these phases from the simple oxides. In addition, due to the scarcity of phase equilibria data for these complex and high-order systems, we considered only the hollandite phase in this work. The DFT results indicate that actinide-bearing hollandites can be stable. However, competing phases may also be present in the same compositional region, potentially limiting or reducing the stability of the predicted compounds to some extent. This necessitates further experimental exploration.

CRediT authorship contribution statement

Amir M. Mofrad: Writing – original draft, Methodology, Investigation, Formal analysis, Data curation, Conceptualization. **Matthew S. Christian:** Writing – review & editing, Methodology, Investigation. **Juliano Schorne-Pinto:** Methodology, Investigation, Conceptualization. **Jake Amoroso:** Investigation, Funding acquisition, Conceptualization. **Kyle S. Brinkman:** Writing – review & editing, Methodology, Investigation. **Hans-Conrad zur Loye:** Writing – review & editing, Investigation, Funding acquisition, Conceptualization. **Theodore M. Besmann:** Writing – review & editing, Investigation, Funding acquisition, Conceptualization.

Declaration of competing interest

The authors declare that they have no known competing financial interests or personal relationships that could have appeared to influence the work reported in this paper.

Data availability

Data will be made available on request.

Declaration of generative AI and AI-assisted technologies in the writing process

During the preparation of this work the author(s) used ChatGPT in order to correct grammar errors and improve readability. After using this tool/service, the author(s) reviewed and edited the content as needed and take(s) full responsibility for the content of the publication.

Acknowledgements

The authors acknowledge the support of the Center for Hierarchical Waste Form Materials, an Energy Frontier Research Center funded by the US Department of Energy, Office of Science, Basic Energy Sciences (DE-SC0016574). Computations in this work were performed (i) using the Extreme Science and Engineering Discovery Environment (XSEDE) [37], which is supported by the National Science Foundation under the grant number ACI-1548562 (through allocation TG-CHE210005) and (ii) the high-performance computing cluster, Hyperion, supported by the Division of Information Technology at the University of South Carolina.

References

[1] H.-C. zur Loye, T. Besmann, J. Amoroso, K. Brinkman, A. Grandjean, C.H. Henager, S. Hu, S.T. Misture, S.R. Phillpot, N.B. Shustova, H. Wang, R.J. Koch, G. Morrison, E. Dolgopolova, Hierarchical materials as tailored nuclear waste forms: a perspective, Chem. Mater. 30 (14) (2018) 4475–4488, https://doi.org/10.1021/acs.chemmater.8b00766.

[2] H. Abe, A. Satoh, K. Nishida, E. Abe, T. Naka, M. Imai, H. Kitazawa, Electrochemical immobilization of cs in single-crystalline synroc, J. Solid State Chem. 179 (5) (2006) 1521–1524, https://doi.org/10.1016/j.jssc.2006.02.005, http://www.sciencedirect.com/science/article/pii/S0022459606000946.

[3] K.J. Nikula, B.A. Muggenburg, W.C. Griffith, W.W. Carlton, T.E. Fritz, B.B. Boecker, Biological effects of ^{137}cscl injected in beagle dogs of different ages, Radiat. Res. 146 (5) (1996) 536–547, http://www.jstor.org/stable/3579554.

[4] V. Aubin-Chevaldonnet, D. Caurant, A. Dannoux, D. Gourier, T. Charpentier, L. Mazerolles, T. Advocat, Preparation and characterization of (Ba,Cs)(M,Ti)_8O_16 (M=Al_3+, Fe_3+, Ga_3+, Cr_3+, Sc_3+, Mg_2+) hollandite ceramics developed for radioactive cesium immobilization, J. Nucl. Mater. 366 (1) (2007) 137–160, https://doi.org/10.1016/j.jnucmat.2006.12.051, http://www.sciencedirect.com/science/article/pii/S0022311507000086.

[5] W.M. Lee, M.I. Ojovan, M.C. Stennett, N.C. Hyatt, Immobilisation of radioactive waste in glasses, glass composite materials and ceramics, Adv. Appl. Ceram. 105 (1) (2006) 3–12, https://doi.org/10.1179/174367606X81669.
[6] J.W. Amoroso, J. Marra, C.S. Dandeneau, K. Brinkman, Y. Xu, M. Tang, V. Maio, S.M. Webb, W.K. Chiu, Cold crucible induction melter test for crystalline ceramic waste form fabrication: a feasibility assessment, J. Nucl. Mater. 486 (2017) 283–297, https://doi.org/10.1016/j.jnucmat.2017.01.028.
[7] A. Ringwood, S. Kesson, N. Ware, W. Hibberson, A. Major, Immobilisation of high level nuclear reactor wastes in synroc, Nature 278 (5701) (1979) 219–223.
[8] D.M. Levins, R.S.C. Smart, Effects of acidification and complexation from radiolytic reactions on leach rates of SYNROC C and nuclear waste glass, Nature 309 (5971) (1984) 776–778.
[9] R. Grote, M. Zhao, L. Shuller-Nickles, J. Amoroso, W. Gong, K. Lilova, A. Navrotsky, M. Tang, K. Brinkman, Compositional control of tunnel features in hollandite-based ceramics: structure and stability of $(Ba,Cs)_{1.33}(Zn,Ti)_8\ O_{16}$, J. Mater. Sci. 54 (2) (2019) 1112–1125.
[10] R. Grote, T. Hong, L. Shuller-Nickles, J. Amoroso, M. Tang, K. Brinkman, Radiation tolerant ceramics for nuclear waste immobilization: structure and stability of cesium containing hollandite of the form (Ba,Cs)_1.33(Zn,Ti)_8O_16 and (Ba,Cs)1.33(Ga,Ti)8O16, J. Nucl. Mater. 518 (2019) 166–176, https://doi.org/10.1016/j.jnucmat.2019.03.005, http://www.sciencedirect.com/science/article/pii/S002231151831540X.
[11] T.-Y. Chen, E.R. Maddrell, N.C. Hyatt, J.A. Hriljac, A potential wasteform for Cs immobilization: synthesis, structure determination, and aqueous durability of Cs_2TiNb_6O_18, Inorg. Chem. 55 (24) (2016) 12686–12695, https://doi.org/10.1021/acs.inorgchem.6b01826.
[12] S.A. Utlak, T.M. Besmann, K.S. Brinkman, J.W. Amoroso, Thermodynamic assessment of the hollandite high-level radioactive waste form, J. Am. Ceram. Soc. 102 (10) (2019) 6284–6297, https://doi.org/10.1111/jace.16438.
[13] M. Tang, P. Tumurugoti, B. Clark, S. Sundaram, J. Amoroso, J. Marra, C. Sun, P. Lu, Y. Wang, Y.-B. Jiang, Heavy ion irradiations on synthetic hollandite-type materials: Ba_1.0Cs_0.3A_2.3Ti_5.7O_16 (A = Cr, Fe, Al), J. Solid State Chem. 239 (2016) 58–63, https://doi.org/10.1016/j.jssc.2016.04.014, http://www.sciencedirect.com/science/article/pii/S0022459616301372.
[14] K. Momma, F. Izumi, VESTA3 for three-dimensional visualization of crystal, volumetric and morphology data, J. Appl. Crystallogr. 44 (6) (2011) 1272–1276, https://doi.org/10.1107/S0021889811038970.
[15] J.E. Post, R.B. Von Dreele, P.R. Buseck, Symmetry and cation displacements in hollandites: structure refinements of hollandite, cryptomelane and priderite, Acta Crystallogr., Sect. B 38 (4) (1982) 1056–1065, https://doi.org/10.1107/S0567740882004968.
[16] S. Kesson, T. White, Radius ratio tolerance factors and the stability of hollandites, J. Solid State Chem. 63 (1) (1986) 122–125, https://doi.org/10.1016/0022-4596(86)90160-X, http://www.sciencedirect.com/science/article/pii/002245968690160X.
[17] Y. Xu, Y. Wen, R. Grote, J. Amoroso, L.S. Nickles, K.S. Brinkman, A-site compositional effects in ga-doped hollandite materials of the form $Ba_xCs_yGa_{2x+y}Ti_{8-2x-y}O_{16}$: implications for Cs immobilization in crystalline ceramic waste forms, Sci. Rep. 6 (2016) 27412.
[18] Y. Wen, Y. Xu, K.S. Brinkman, L. Shuller-Nickles, Atomistic scale investigation of cation ordering and phase stability in Cs-substituted $Ba_{1.33}Zn_{1.33}Ti_{6.67}O_{16}$, $Ba_{1.33}Ga_{2.66}Ti_{5.67}o_{16}$ and $Ba_{1.33}Al_{2.66}Ti_{5.33}O_{16}$ hollandite, Sci. Rep. 8 (1) (2018) 1–11.
[19] M. Zhao, J.W. Amoroso, K.M. Fenker, D.P. DiPrete, S. Misture, S. Utlak, T. Besmann, K. Brinkman, The effect of cesium content on the thermodynamic stability and chemical durability of $(Ba, Cs)_{1.33}(Al, Ti)_8O_{16}$ hollandite, J. Am. Ceram. Soc. 103 (12) (2020) 7310–7321.
[20] P. Hohenberg, W. Kohn, Inhomogeneous electron gas, Phys. Rev. 136 (1964) B864–B871, https://doi.org/10.1103/PhysRev.136.B864, https://link.aps.org/doi/10.1103/PhysRev.136.B864.
[21] W. Kohn, L.J. Sham, Self-consistent equations including exchange and correlation effects, Phys. Rev. 140 (1965) A1133–A1138, https://doi.org/10.1103/PhysRev.140.A1133, https://link.aps.org/doi/10.1103/PhysRev.140.A1133.
[22] G. Kresse, J. Hafner, Ab initio molecular dynamics for liquid metals, Phys. Rev. B 47 (1993) 558–561, https://doi.org/10.1103/PhysRevB.47.558, https://link.aps.org/doi/10.1103/PhysRevB.47.558.
[23] G. Kresse, J. Hafner, Ab initio molecular-dynamics simulation of the liquid-metal–amorphous-semiconductor transition in germanium, Phys. Rev. B 49 (1994) 14251–14269, https://doi.org/10.1103/PhysRevB.49.14251, https://link.aps.org/doi/10.1103/PhysRevB.49.14251.
[24] G. Kresse, J. Furthmüller, Efficiency of ab-initio total energy calculations for metals and semiconductors using a plane-wave basis set, Comput. Mater. Sci. 6 (1) (1996) 15–50, https://doi.org/10.1016/0927-0256(96)00008-0, https://www.sciencedirect.com/science/article/pii/0927025696000080.
[25] G. Kresse, J. Furthmüller, Efficient iterative schemes for ab initio total-energy calculations using a plane-wave basis set, Phys. Rev. B 54 (1996) 11169–11186, https://doi.org/10.1103/PhysRevB.54.11169, https://link.aps.org/doi/10.1103/PhysRevB.54.11169.
[26] F. Bloch, Nuclear induction, Phys. Rev. 70 (1946) 460–474, https://doi.org/10.1103/PhysRev.70.460, https://link.aps.org/doi/10.1103/PhysRev.70.460.
[27] G. Kresse, D. Joubert, From ultrasoft pseudopotentials to the projector augmented-wave method, Phys. Rev. B 59 (3) (1999) 1758–1775.
[28] J.P. Perdew, A. Zunger, Self-interaction correction to density-functional approximations for many-electron systems, Phys. Rev. B 23 (1981) 5048–5079, https://doi.org/10.1103/PhysRevB.23.5048, https://link.aps.org/doi/10.1103/PhysRevB.23.5048.
[29] J.P. Perdew, K. Burke, M. Ernzerhof, Generalized gradient approximation made simple, Phys. Rev. Lett. 77 (18) (1996) 3865–3868.
[30] A. Jain, S.P. Ong, G. Hautier, W. Chen, W.D. Richards, S. Dacek, S. Cholia, D. Gunter, D. Skinner, G. Ceder, K.A. Persson, Commentary: the materials project: a materials genome approach to accelerating materials innovation, APL Mater. 1 (1) (2013) 011002, https://doi.org/10.1063/1.4812323.
[31] S. Kirklin, J.E. Saal, B. Meredig, A. Thompson, J.W. Doak, M. Aykol, S. Rühl, C. Wolverton, The open quantum materials database (OQMD): assessing the accuracy of DFT formation energies, npj Comput. Mater. 1 (1) (2015) 1–15.
[32] H.J. Monkhorst, J.D. Pack, Special points for Brillouin-zone integrations, Phys. Rev. B 13 (12) (1976) 5188–5192.
[33] S.L. Dudarev, G.A. Botton, S.Y. Savrasov, C.J. Humphreys, A.P. Sutton, Electron-energy-loss spectra and the structural stability of nickel oxide: an LSDA+U study, Phys. Rev. B 57 (1998) 1505–1509, https://doi.org/10.1103/PhysRevB.57.1505.
[34] M. Zhao, Y. Xu, L. Shuller-Nickles, J. Amoroso, A.I. Frenkel, Y. Li, W. Gong, K. Lilova, A. Navrotsky, K.S. Brinkman, Compositional control of radionuclide retention in hollandite-based ceramic waste forms for cs-immobilization, J. Am. Ceram. Soc. 102 (7) (2019) 4314–4324.
[35] M. Zhao, N. Birkner, J. Schaeperkoetter, R.J. Koch, P. Russell, S.T. Misture, T.M. Besmann, J. Amoroso, K.S. Brinkman, Durable Cr-substituted $(Ba, Cs)_{1.33}(Cr, Ti)_8O_{16}$ hollandite waste forms with high Cs loading, J. Am. Ceram. Soc. 105 (6) (2022) 4564–4576.
[36] M. Zhao, P. Russell, J. Amoroso, S. Misture, S. Utlak, T. Besmann, L. Shuller-Nickles, K.S. Brinkman, Exploring the links between crystal chemistry, cesium retention, thermochemistry and chemical durability in single-phase $(Ba, Cs)_{1.33}(Fe, Ti)_8O_{16}$ hollandite, J. Mater. Sci. 55 (2020) 6401–6416.
[37] J. Towns, T. Cockerill, M. Dahan, I. Foster, K. Gaither, A. Grimshaw, V. Hazlewood, S. Lathrop, D. Lifka, G.D. Peterson, R. Roskies, J.R. Scott, N. Wilkins-Diehr, Xsede: accelerating scientific discovery, Comput. Sci. Eng. 16 (5) (2014) 62–74, https://doi.org/10.1109/MCSE.2014.80.